Concrete Subsurface Crack Detection Using Thermal Imaging in a Deep Neural Network

Dr Mabrouka Abuhmida*[1], Daniel Milner[2], Assoc-Prof Jiping Bai[3]
[1,2,3]University of South Wales
E-mail: ***[1]Mabrouka.abuhmida@southwales.ac.uk**, [2]Daniel.milner@southwales.ac.uk , [3]Jiping.bai@southwales.ac.uk

Abstract

Impact actions, such as a zone directly affected by conflict and warfare, can negatively impact the structural integrity of concrete structures. Even indirect impact actions can make structures unsafe, creating subsurface defects in concrete. However, the result of indirect impact actions is often undetected because of the time required and expert knowledge needed to assess the structure. Yet, there are no techniques currently available to assess the usability and the safety of a concrete structure rapidly and with no expert knowledge.. This paper presents a combination of thermal imaging and artificial intelligence (AI) to enable a novel, contactless, autonomous, and fast technique for detecting hidden defects in concrete structures. In this paper, a ResNet50 model was trained on simulated data of subsurface defected and defect-free concrete blocks to test if it is possible to classify between the two. The model developed achieved a validation accuracy of 99.93%. Because of the success of this model, a laboratory experiment was conducted by compressing concrete blocks and recording the process using a thermal camera to create a dataset of concrete blocks with and without subsurface cracks. This dataset was used to train a new model with the same architecture and hyper-parameters as the initial model and achieved a validation accuracy of 100%. This investigation proves it is possible for AI to detect subsurface cracks and hidden defects by classifying the thermal images of concrete surfaces.

Keywords— *Deep learning, thermal imaging, concrete defects, artificial intelligence.*

1. Introduction

Like any other built environment, concrete structures must be tested and monitored to assess their structural integrity. Ideally, structural testing is performed without damaging the structure using a non-destructive testing (NDT) technique such as sonic, ultrasonic, ground penetrating radar (GPR), microwaves, infrared thermography, or radiography [1]. Also, partially destructive testing (PDT) techniques are commonly used where a minor level of damage is required, such as surface hardness, penetration resistance testing, pull-out and pull-off, and break-off testing methods. Destructive testing (DT) techniques involve taking samples of the structure's material for off-site testing in the laboratory, such as the popular method of coring [2]

DT techniques are costly methods [3], [4] and inadequate when the testing needs to be rapid [5]. Both PDT and DT techniques require repairs that make testing even more impractical for non-experts. For these reasons, this study focuses on a potential advancement in the NDT field and investigates producing quantitative results that substitute those generated from DT

methods. The range of properties that can be assessed using NDT is large. It includes fundamental parameters such as density, elastic modulus, strength, surface hardness, and surface absorption [4]. In some NDT cases, it is possible to detect voids, cracking, and delaminations in the concrete that can be easily missed in most DT and PDT methods [2].

Sometimes surface-level defects indicate that structural safety tests must be performed on a concrete structure. There can be unsafe concrete structures because of subsurface-level defects that cannot be easily detected by a civilian or expert, sometimes indicating no justification for concrete testing [6]. This is particularly concerning given that structural assessment of concrete structures is generally ignored outside of the area affected by impact action, which is a zone directly affected by conflict and warfare [7]. Areas directly affected by impact action typically give a visible indication for performing a safety test, such as surface-level cracks. However, areas that are indirectly affected by impact activities, such as a few metres away from a detonation site, may provide no visual indication for performing a safety test yet have subsurface-level defects that create structural safety concerns. Although near an area of impact action, an expert may be unwilling to carry out a structural safety test due to less likelihood of structural damage than in areas directly affected by impact action [8]. An expert to carry out a test for someone concerned can also be expensive, and training, equipment, and safety concerns make a civilian performing the test impractical. The indirect effect of impact action can affect structures that put many people at risk, such as homes, schools, and hospitals.

Aside from the issues of practicality previously discussed, conventionally employed techniques for NDT of concrete require non-remote, contact-based, and experienced professionals to perform the test and interpret the data, which are issues that this study aims to address. This paper uses a thermal imaging technique as an alternative approach for contactless NDT of concrete for detecting subsurface defects by measuring the temperatures at the material's surface. In thermal imaging, the regions of defects have different densities, heat capacities, and heat conductivities compared to the surrounding concrete and thus get differentiated out and identified [8], [9], [10]. This act of identification would be time-consuming and difficult for an expert and so is replaced by an artificial intelligence (AI) system trained on a large dataset of normal and defected concrete (see section \ref{dataset}). AI has been used in many studies to enhance the identification process [11], [12], [13], [14]. And combining this with thermal imaging's ability to be upscaled to evaluate a large part of a structure makes this technique significantly more time sufficient than any current NDT, PDT, or DT technique.

Thermography enables the real-time detection and measurement of temperature by detecting infrared (IR) light, which has a wavelength ranging between 800 nm and 1 mm on the electromagnetic spectrum [15]. Thermal images come in various formats, such as jet, greyscale, and overlay. Although these images appear different, all represent the temperature at each pixel's position [16]. The pros of thermal imaging include high portability, non-contact temperature measurement, and the absence of harmful radiation [17]. Recording thermal images require prerequisites for accurate measurements:

- Emissivity scaled between 0 and 1. Total emissivity (1) occurs when the thermal radiation of the target is 100. And zero emissivity (0) occurs when the thermal radiation of the target is 0. An
- An emissivity of 1 gives the most accurate representation of the target's surface temperature.
- Emissivity for concrete is an average emissivity of 0.95 [18].
- The distance from the camera to the target is typically one metre.
- The room temperature was recorded at 20 °C.

1.1 Related Work

The literature contains a wealth of valuable citations that cover several applications of the thermal imaging technique in civil structures, such as determining the degree of thermal insulation, detecting internal moisture, and locating buried pipelines. Sakagami and Kubo [19] introduced lock-in thermography to detect delamination in concrete. And could successfully detect defects of the order of 10 mm in length. Maierhofer et al. [20] also succeeded in locating defects through-thickness crack of 50 mm in width using impulse thermography and presented numerical studies to determine the depth of the defects based on the time of occurrence of the maximum temperature difference. Wiggenhauser used cooling-down thermography to identify subsurface structural deficiencies [21].

Cheng et al. [22]used the synthesis of information gathered from active infrared thermography (IRT) and elastic waves to inspect building exteriors. Other reviews described several related works to the application of thermal imaging techniques can be found in publications such as [23] and [10].

Youngjun Cho et al. in [24] have introduced a deep thermal imaging approach for close-range automatic materials recognition utilising a low-cost mobile thermal camera integrated into a smartphone to capture thermal textures. Their proposed deep neural network classifier succeeded in classifying these textures into material types, and their contactless approach was effective without the need for ambient light sources. A total of 32 material types in indoor and outdoor environments were evaluated, and their system approximates a confidence of 98% in 14,860 images of 15 indoor materials and above 89% in 26,584 images of 17 outdoor materials. Their results are very promising and impactful in a way that, even with less feature engineering, deep learning coupled with thermal imaging can identify trends in the fed data. When applied to our approach, this means that the system has a great chance of identifying anomalies in concrete structures with little done towards feature extractions, and the system will be capable of learning complex patterns in the thermal dataset.

The following sections will discuss in detail the most influential papers related to this work.

1.1.1 Effects of High Temperature on the Properties of High-Performance Concrete (HPC) [25]

This investigation aims to understand heat's effect on concrete by simulating concrete exposed to fire. It begins by discussing how heat has been found to reduce the concrete's strength. For example, as temperature exposure increases, compressive strength, tensile strength and elasticity decrease. The researchers aim to prove these past findings by heating concrete blocks up to 600 °C in an oven and then testing multiple strength parameters to create strength-heat curves. This study highlights how fire-exposed concrete can have many negative consequences that could result in concrete structures being safety risks. It also highlights the importance of being able to detect such defects.

1.1.2 Deep Learning-Based Thermal Crack Detection on Structural Concrete Exposed to Elevated Temperature [26]

It is discussed that environmental factors, fatigue stress, and heavy loading are some common causes of cracks in structural concrete and improper maintenance or lack of inspections reinforce structural deterioration. This investigation aims to overcome the limitations of past research by utilising the novel method of pixel-level-based crack segmentation of RGB images of cracks in concrete exposed to fire. A U-Net architecture trained on 200 greyscale concrete-cracked photographs is used, encompassing the encoder-decoder framework. Within the encoder part of the framework, features extracted from the image are

used as input and in the decoder part, features are fused and up-sampled to create a crack-segmented image of the concrete. Concrete specimens of size 150 x 150 x 150 mm were cracked through exposure to elevated temperature for the heating duration of 30 min at 821°C, 60 min at 925°C, 90 min at 986°C, 120 min at 1029°C, 150 min at 1059°C, 180 min at 1090°C, 210 min at 1111°C and 240 min at 1133°C as per the standard fire curve. The standard fire curve represents the thermal energy created during a standard fire over time. The Intersection over Union, a common measurement of image segmentation accuracy of 78.12% and model accuracy of 99.74%, was achieved. This study enabled location detection of minor and major cracks. However, it needs more data to be generalisable to other concrete structures and is limited to surface-level cracks. This study highlights one of a multitude of ways in which AI can be successfully used for crack detection in an NDT method. The causes for cracks listed within this paper imply that the effects of impact action are sometimes overlooked, and there is a lack of structural safety inspections that could prevent further structural deterioration that this study and our study aim to address.

1.1.3 Multivariate Analysis of Concrete Image Using Thermography [9]

Image analysis can give indications of the health condition of a concrete structure. This study implements two AI systems, a Convolutional Neural Network (CNN) trained on 2,700 images and Support Vector Machine (SVM) in a proof of concept that could be deployed in an automated system to detect major damage, such as visible cracks in concrete structures. Thermal images were captured of cracked and non-cracked concrete on various structures at universities in Daegu City, Republic of Korea. The images were enhanced using various computer vision techniques. The proof of concept developed can classify concrete cracks in thermal images with an accuracy of 98%. This study highlights the growing demand for structural health monitoring systems while also showing how thermal imaging can be a solution more effective than RGB imaging.

1.1.4 NDT Approach for Characterisation of Subsurface Cracks in Concrete [27]

Thermal imagery can be extremely useful in detecting cracks, especially given the large sizes of concrete structures. It can even work for subsurface cracks, such as in this study. Concrete defects below the surface affect the heat transfer rate at the structure's surface. In this study, concrete blocks of size 100 x 100 x 400 mm were cracked by four-point bending compression, heated to 60 °C to simulate the sun's heat, and a thermal camera was used to record thermal images of the specimen. The images are viewed to find defects by showing areas of lower temperatures concerning the rest of the concrete block, which is assumed not to be cracked. The thermal imagery is manually analysed to detect signs of a subsurface crack, and then ultrasound is used to measure the depth of the crack, indicating the damage severity. Thermographs captured at 60 °C could reveal vertical subsurface cracks up to 11 mm in depth. This study shows it is possible to use thermal imaging to detect subsurface cracks.

1.1. 5 Influence of Related Work on Study

This related work shows that concrete exposed to impact action creates safety concerns [25]. The publication [9] highlights the growing demand for structural health monitoring systems to detect such concerns. Both [26] and [9] point out that AI can assist the crack detection process, and the authors in [27] make it known that thermal imaging to detect subsurface cracks in concrete is possible. However, no research has been conducted to investigate the possibility of combining the two. This paper is an investigation to find if it is possible to autonomously detect subsurface cracks using thermal images assisted by AI that someone with no expert knowledge in civil engineering could potentially use.

2. Methods

In this study, we employed a combination of thermal imaging and artificial intelligence (AI) to detect hidden defects in concrete structures. The methodology involved two experimental tests: a simulation dataset creation and a laboratory experiment. The following Figure summarises the steps taken to experiment.

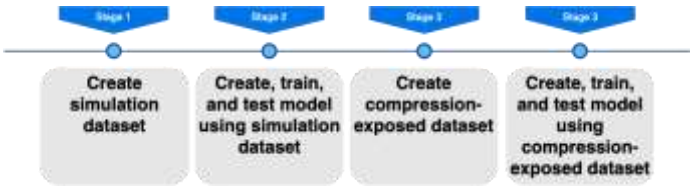

Figure. 1: Stages of the Method

2.1 Simulation Dataset Creation

Before performing costly real-life experiments, a simulation is created using finite element analysis software ABAQUS to create data that will be used to test if an AI system can classify safe and unsafe concrete. [26] have already proven that thermal images can be used to detect subsurface cracks, but the dataset from this experiment is unavailable. From the simulation, a dataset of 12,018 images is created of concrete specimens with and without concrete voids. An example of this is shown in Figure 2, which shows an angled view of the front of the simulated concrete specimens. The specimens have varying dimensions, void dimensions, and temperatures (Table 1).

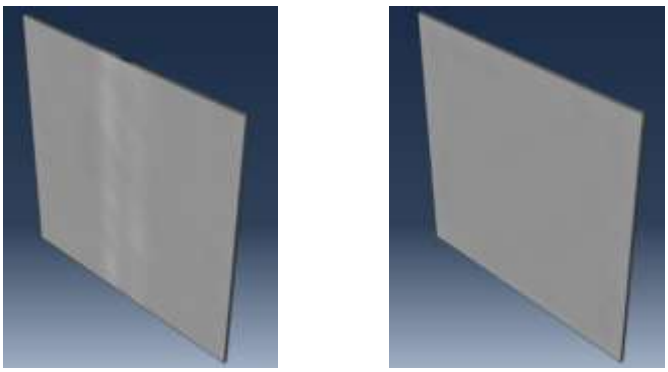

(a) Concrete specimen with subsurface crack

(b) Concrete specimen without subsurface crack

Figure. 2: Thermal Visualisation of Simulated Concrete Blocks

Table 1 Simulation Dataset Description

Dimensions (m)	**Void Dimensions (m)**	**Temp. (°C)**	**Frames**
0.25 x 0.25 x 0.01	0.050 x 0.005	60	501
0.25 x 0.25 x 0.01	0.050 x 0.005	65	501
0.25 x 0.25 x 0.01	0.025 x 0.005	60	501
0.25 x 0.25 x 0.01	0.025 x 0.005	65	501
0.50 x 0.50 x 0.01	0.050 x 0.005	60	501
0.50 x 0.50 x 0.01	0.050 x 0.005	65	501
0.50 x 0.50 x 0.01	0.025 x 0.005	60	501
0.50 x 0.50 x 0.01	0.025 x 0.005	65	501
0.75 x 0.75 x 0.01	0.050 x 0.005	60	501
0.75 x 0.75 x 0.01	0.050 x 0.005	65	501
0.75 x 0.75 x 0.01	0.025 x 0.005	60	501
0.75 x 0.75 x 0.01	0.025 x 0.005	65	501
0.25 x 0.25 x 0.01	No Void	60	1001
0.25 x 0.25 x 0.01	No Void	65	1001
0.50 x 0.50 x 0.01	No Void	60	1001
0.50 x 0.50 x 0.01	No Void	65	1001
0.75 x 0.75 x 0.01	No Void	60	1001
0.75 x 0.75 x 0.01	No Void	65	1001

Each specimen begins with an ambient temperature of 0 °C, and a transient heat flux of 60 °C is applied at the rear of the panel to simulate sunrise like in [27]. The simulation results are set to consist of 500 steps for the specimens with a void, meaning 501 frames of the front of the specimen are exported in video format from ABAQUS. Five hundred steps, where each step is one second, are used to provide sufficient iterations to allow the specimen's thermal properties to change and plateau. The frames show the front side of the ABAQUS model in greyscale with a fixed temperature scale with nodes at multiple areas of the model having variable temperature values; more can be found in the publicly available dataset [28]. And an example of the images used to train the model is shown in Figure 3. As there are fewer variations of parameters for the void-free specimens, the simulation is set to consist of 1000 steps, meaning 1,001 frames of the front of the specimen are exported in video format from ABAQUS. For each simulation, the video is cropped to fit the specimen only, and each frame is exported.

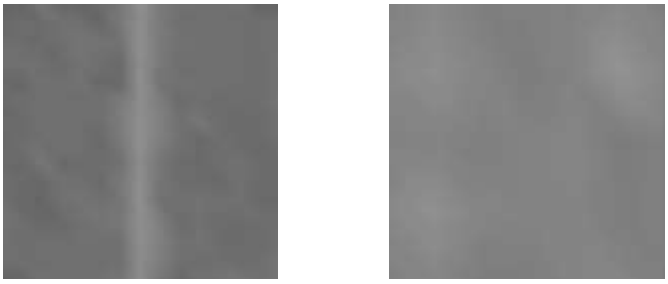

(a) Concrete specimen with subsurface crack

(b) Concrete specimen without subsurface crack

Figure. 3: Examples from the Dataset Used to Train the Model

2.4 Camera and Specimen Preparation

The specifications for the thermal imaging camera used are given in Table 2. The camera is set to record in colour, meaning there is the choice to change the format to greyscale should it be needed later. As few on-screen parameters as possible are enabled to aid in creating a clean dataset. The concrete blocks have been The concrete blocks, water cured for 28 days and have the standard dimensions of 100 x 100 x 100 mm for strength tests. The cement content in the mixtures was replaced with pulverised-fuel ash (PFA) at 10, 20 and 30% levels.

Table 2: Thermal Camera Technical Specifications

Parameter	**Hikmicro G60**
Field of View	25° × 19°
Temperature Measurement Range	-20 °C to 650 °C
Image Frequency	9 Hz
Accuracy	Max (±2°C, ±2%)
Image File Format	BMP
Video File Format	MP4
Resolution	640 x 512

2.5 Compression-exposed Concrete Data Collection

Was followed it was confirmed that the model could classify thermal images with and without voids. First, a concrete specimen was loaded into the compression machine, and a thermal imaging camera was set up one meter away on a tripod to face it. The emissivity of the camera was set to 0.95, and the room temperature was recorded and set at 20°C. Then, the recording was initiated, and pressure was gradually applied to the specimen using the pressure machine until visible cracks were formed. Once cracks became apparent, the recording was stopped. This process was repeated eight times on concrete specimens to create a large dataset. The following summarises the laboratory experiment:

1) A specimen was loaded into the compression machine, and the thermal imaging camera was setup one metre away on a tripod to face it. The emissivity is set to 0.95, and the room temperature is recorded at 20 °C.
2) Once recording began, the pressure was gradually applied to the specimen using the pressure machine up to the amount of force required to create visible cracks.
3) The recording is stopped once cracks are clearly visible.
4) This process was performed eight times on concrete specimens to create a large dataset.

Each video recording from the data collection phase is, on average, two minutes long, and then unnecessary data is removed and, through visual inspection, is split to create two sub-videos comprising thermal captures of non-cracked concrete and subsurface-cracked concrete only. As the data is now separated into two classes, the video frames are extracted to create an image dataset. Blurred and similarly unclean data is removed to reduce the anomalies in the dataset. The images are grayscale to reduce training time, improve generalisation, and avoid local minima; each image is normalised to between zero and one.

Figure 5 shows the image for the specimen with no defects before applying pressure 5-An and with cracks forming while applying pressure 5B, C and D. The minimum temperature in this image is around 19 °C, and the maximum temperature is around 63.5 °C. In the processed image, we used 255 different thresholds, known as grey thresholds, and each of these thresholds is assigned to a specific temperature. The dataset for the compression-exposed concrete data can be found in [38].

(a) None (b) Invisible (c) Visible (d) Obvious

Figure. 5: Specimen Thermal Image Showing Defects

2.6 AI Model Construction for Real-Life Thermal Dataset

The AI model trained on the simulation dataset is reused for the laboratory experiment. However, the data used for the model training is replaced with 11,145 thermal images captured from the laboratory experiment. This dataset comprises 5,651 thermal images of uncracked concrete specimens and 5,494 thermal images of cracked concrete specimens. The ResNet50 model and hyper-parameters are identical to those used for the simulation dataset. The training process took a total of 37.75 minutes to complete.

2.7 AI Model Construction for Simulation Dataset

The ResNet50, a convolutional neural network (CNN) model, is created and trained using TensorFlow version 2.7.0 to classify the specimens with and without a void using the simulation dataset. The ResNet model has an extremely deep architecture [29]. Mainly composed of residual blocks, meaning nodes in the neural network can jump between and skip layers, unlike shallow networks where consecutive hidden layers are linked to each other [30].
The main compelling advantages of the residual connections in the ResNet architecture are that the connections preserve the gained knowledge during training and speed up the training time of the model by increasing the network capacity [31].

In this experiment, a ResNet50 model was used to classify thermal images of concrete structures with and without subsurface defects. ResNet50 is a type of convolutional neural network (CNN) that has been widely used in image classification tasks due to its deeper architecture and superior performance compared to other CNNs [32]. The ResNet50 model consists of 48 Convolution layers along with one max pool and one Average Pool layer [33], [34]. This model has 23,585,538 parameters, 23,532,418 trainable parameters, and 53,120 non-trainable parameters. The input size is (256 x 256 x 1), which means that the input images are grayscale. The model was trained for twenty epochs, taking 37.35 minutes, using a train-test split where 25% of the data is reserved for testing, a batch size of eight, a learning rate of 0.001, and using the Adam optimiser.

Compared to other pre-trained models such as VGG and Inception, ResNet50 has been shown to outperform them on various image classification tasks [35], [36]. ResNet50 has also been shown to be efficient in extracting features from images, making it a suitable model for detecting subsurface defects in concrete structures from thermal images [37]. Therefore, ResNet50 was chosen as the model of choice for this experiment due to its superior performance in image recognition tasks, particularly in the domain of subsurface defect detection in concrete structures from thermal images.

In this experiment, the hardware used to train the model is a 10GB NVIDIA GEFORCE RTX 3080 GPU, AMD Ryzen 9 5900X 12 Core CPU (3.7GHz-4.8GHz/70MB CACHE/AM4), and 64GB DDR4 3200MHz RAM; the GPU is selected for model training. Once trained, at epoch sixteen, the model achieved an accuracy of 0.9992, validation accuracy of 0.9993, loss of 0.0024, and validation loss of 0.0015. When testing against an unseen dataset for a void-free simulation of new dimensions of 0.37 x 0.37 x 0.01 m and temperature at the rear of 60 °C, the system correctly predicted 501 of 501 frames. When testing against an unseen dataset for a simulation including a void of size 0.0125 mm, half the size of the smallest void dimension the AI has been trained for, the system predicted 500 of 501 frames correctly.

2.7.1 Model functions

The code is designed to classify two types concrete images:

- (unsafe, 1) and'
- without a void (safe, 0).

Using both the simulated data and the laboratory data one at the time.

The code extracts frames from the videos, pre-processes them, trains a deep learning model, and then classifies the images based on whether they are safe or unsafe.

Here is an overview of each section and the functions used:

Imports: Import necessary libraries for data manipulation, pre-processing, and deep learning model training. Libraries include *os, random, imageio, PIL, cv2, matplotlib, pandas, numpy, tensorflow, and sklearn.*

Load a Test Image: This commented section demonstrates how to load and visualize a test CSV image. It reads the CSV file, checks the size and shape of the data, and finds the lowest and highest temperature values. It then visualizes the temperature data using a colormap.

Pre-process all Data:

- Define image dimensions (*width and height*) for resizing images.
- *Extract frames from videos*: Read the videos using *cv2.VideoCapture*, extract each frame using cv2.read, and save the frames as JPEG images using *cv2.imwrite.*
- *Crop Images*: Read images from a directory, determine their labels (safe/unsafe), and crop the images based on label-specific coordinates.
- Load the Data: Iterate through the directory of processed images and read them using *cv2.imread*. Assign labels (0 or 1) based on the file name.
- Normalize Data: Convert the image and label data to *NumPy* arrays and normalize the image data by dividing by 255.
- *Check Data Balance*: Count the number of samples for each class and plot the distribution using a bar chart.
- *Save and Load X and y*: Save the processed image and label data as *NumPy* arrays and load them for further use.

The following code shows the images normalisation method.

```
[ ]  X = np.array(X)
     y = np.array(y)
     X = X.astype('float32') / 255.
     y = y.astype('int')
     print("X:")
     print("Samples: {}, Type: {}, Shape: {}".format(len(X), X.dtype, X[0].shape))
     print()
     print("Y:")
     print("Samples: {}, Type: {}".format(len(y), y.dtype))
```

```
X:
Samples: 202, Type: float32, Shape: (128, 128, 3)

Y:
Samples: 202, Type: int32
```

Code. 1: Display Some Images

Display Some Images: Display random images and their labels from the dataset. Use a jet colormap to visualize the images. The Code X shows the function method.

```
# plot random images and their labels
names = ['Safe (0)','Unsafe (1)']
print(X[0].shape)
plt.figure(figsize=(10,10))
for i in range(len(names)):
    ax = plt.subplot(1, 3, i+1)
    rnd = random.randint(0, len(X))
    img = cv2.resize(X[rnd], dims)
    plt.jet()
    plt.imshow(img)
    plt.title("{} - {}".format(y[rnd], names[int(y[rnd])]))
    ax.get_xaxis().set_visible(False)
    ax.get_yaxis().set_visible(False)
plt.show()
```

```
(128, 128, 3)
```

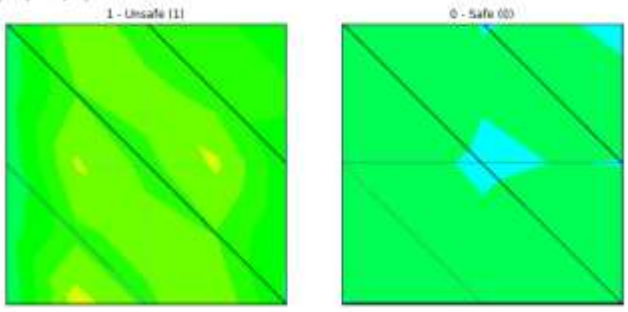

Code. 2: Display Some Images

Create Test-Train Split: Use train_test_split from sklearn.model_selection to split the dataset into training and testing sets.

Setup and Run Model:

- Define the deep learning model architecture (ResNet50) using TensorFlow Keras. Set input shape and number of output classes.
- Compile the model using the Adam optimizer, Sparse Categorical *Crossentropy* loss, and accuracy metric.
- Define a custom *callback* class *Save_CB* to save the model in different formats *(.pb and .h5)* at the end of each epoch.

- Train the model using *model.fit*, providing training data, batch size, number of epochs, validation data, verbosity level, and the custom *callback*.
- Plot the training results, including loss and accuracy comparisons between training and validation sets.

The following Code shows the Model code:

```
#model = keras.backend.set_image_data_format('channels_first')
keras.backend.set_image_data_format('channels_last')
model = tf.keras.applications.resnet50.ResNet50(include_top=True,
                                                weights=None,
                                                input_tensor=None,
                                                input_shape=(height, width, 3),
                                                pooling=None,
                                                classes=2)
model.summary()
```

Code. 3: ResNet50 Setup

Predict on a Test Image: Use the trained model to predict the class of a test image, visualize the result, and display the actual and predicted labels.

Load Model: Load a previously saved model using *tf.saved_model.load* to use for prediction.
Throughout the code, various functions from the imported libraries are used to perform tasks such as reading and writing images, resizing images, and splitting data into training and testing sets. The deep learning model used in this code is ResNet50, a popular convolutional neural network architecture for image classification.

Because the model achieved such high accuracy, hyper-parameter optimisation was not performed because, after testing, only very minor gains could be made, which are insignificant, especially for a proof-of-concept project such as this. The analysis of the model's performance using both simulated and lab data is shown in Figure 4.

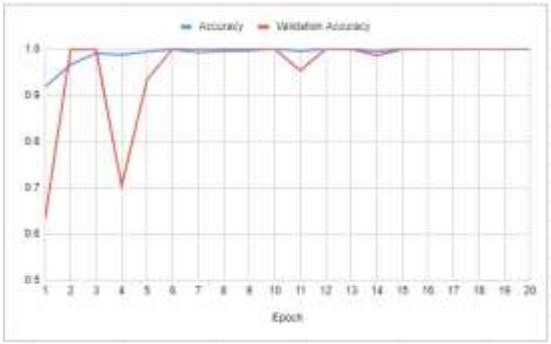

(a) Accuracy vs validation accuracy - laboratory data

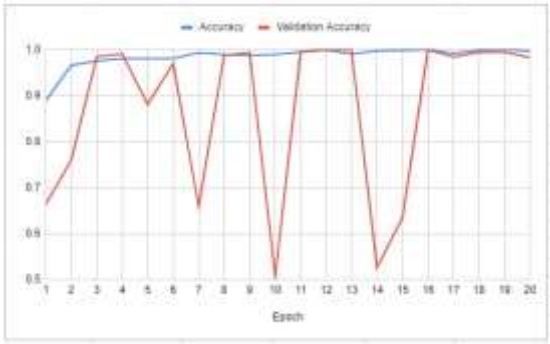

(b) Accuracy vs validation accuracy - simulation data

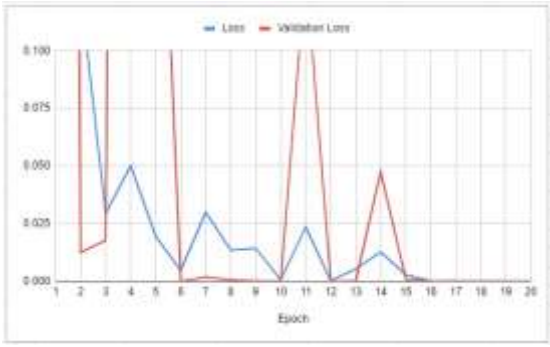

(c) Loss vs validation loss - laboratory data

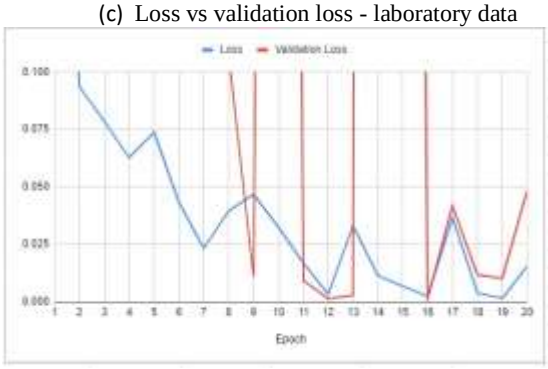

(d) Loss vs validation loss - simulation data

Figure. 4: Model Performance During Training

3. RESULTS AND DISCUSSION

3.1 AI Model Trained on Simulation Dataset

The model trained on the simulated data was very successful at classifying between simulated specimens with and without voids, even when the data contains unseen parameters. Although the unseen dataset with a void did not achieve 100% accuracy, this is likely because it may take some frames to pass before the heat propagates through the specimen to make subsurface cracks visual. This test can be regarded as successful because it was able to classify the majority of the images correctly. The success of this model showed it was possible to classify subsurface defects in concrete, because of this, the remainder of the methodology could be performed. To improve on the simulated dataset, it is recommended that more data from ABAQUS simulations is added with more variation in parameters to improve the generalisability of the model's predictions. For example, the concrete material should be altered to allow for a range of concrete mixes.

3.2. AI Model Trained on Real-Life Thermal Dataset

In total 11,145 frames were captured and used to train the model. After splitting the data to create separate training and testing data and once trained, the model achieved an accuracy of 1.0, validation accuracy of 1.0, loss of 7.0244E-06, and validation loss of 9.4513E-07.

This model was very successful, even without simulation of sunrise or sunset like in [30], meaning when deployed the system can be used without these constraints, making it more accessible. To improve, RGB video should be recorded to 6 provide a side-by-side comparison with the thermal images to show that cracks appearing on the thermal images are subsurface and not visible without the thermal camera. By doing this, it can be ensured that the model is trained on subsurface cracks only.

4. CONCLUSION

In this paper, two experimental tests have been conducted; the first experiment simulates the surface temperature of a concrete structure with and without an existing hidden crack within the structure. The second experiment was performed on a real concrete specimen in a laboratory, where a thermal camera captured thermal changes from zero pressure to the amount required to make cracks visible.

The data from both experiments were used to train two independent AI systems to detect hidden defects autonomously. In conclusion, the technique used in both experiments proved that it is very useful and valid for detecting very small subsurface cracks through thermal images of the surface of concrete blocks. To improve the investigation, additional data should be collected from larger concrete blocks and used to train the model.
This will represent a more typical use-case of a structural wall and increase the generalisability of the predictions. This additional data should also consider the distance between the concrete surface and the subsurface defect; this would enhance the understanding of the capabilities of the system we have developed.

After investigating a range of neural networks to find the fastest and most efficient architecture, we hope this system is fully developed for real-life use by implementing and deploying an AI concrete subsurface defect detector in an easy-to-use and inexpensive hardware component. The technique developed in this research may aid in providing an indication of a

thermal change pattern in very small cracks that could provide insights into larger cracks that could appear before they happen.

REFERENCES

[1] J. C. Agunwamba and T. Adagba, 'A COMPARATIVE ANALYSIS OF THE REBOUND HAMMER AND ULTRASONIC PULSE VELOCITY IN TESTING CONCRETE', *Niger. J. Technol.*, vol. 31, no. 1, p. 9, 2012.

[2] INTERNATIONAL ATOMIC ENERGY AGENCY, 'Guidebook on non-destructive testing of concrete structures'. 2002.

[3] R. L. Wankhade and A. B. Landage, 'Non-destructive Testing of Concrete Structures in Karad Region', *Procedia Eng.*, vol. 51, pp. 8–18, 2013, doi: 10.1016/j.proeng.2013.01.005.

[4] J. Hoła, J. Bień, Ł. Sadowski, and K. Schabowicz, 'Non-destructive and semi-destructive diagnostics of concrete structures in assessment of their durability', *Bull. Pol. Acad. Sci. Tech. Sci.*, vol. 63, no. 1, pp. 87–96, Mar. 2015, doi: 10.1515/bpasts-2015-0010.

[5] G. Thiagarajan, A. V. Kadambi, S. Robert, and C. F. Johnson, 'Experimental and finite element analysis of doubly reinforced concrete slabs subjected to blast loads', *Int. J. Impact Eng.*, vol. 75, pp. 162–173, Jan. 2015, doi: 10.1016/j.ijimpeng.2014.07.018.

[6] M. Valinejadshoubi, A. Bagchi, and O. Moselhi, 'Structural health monitoring of buildings and infrastructure', *Struct. Health Monit.*, vol. 1, p. 50371, 2016.

[7] R. Jankowski, 'Impact force spectrum for damage assessment of earthquake-induced structural pounding', in *Key Engineering Materials*, 2005, vol. 293, pp. 711–718.

[8] C. S. Scutarasu, D. Diaconu-Şotropa, and M. Barbuta, 'Case Study on Modeling Fire Action Complexity in Fire Safety Engineering of Structures', in *Advanced Engineering Forum*, 2017, vol. 21, pp. 102–107.

[9] B. Kim, S.-W. Choi, G. Hu, D.-E. Lee, and R. O. Serfa Juan, 'Multivariate Analysis of Concrete Image Using Thermography and Edge Detection', *Sensors*, vol. 21, no. 21, p. 7396, Nov. 2021, doi: 10.3390/s21217396.

[10] G. F. Sirca Jr. and H. Adeli, 'INFRARED THERMOGRAPHY FOR DETECTING DEFECTS IN CONCRETE STRUCTURES', *J. Civ. Eng. Manag.*, vol. 24, no. 7, pp. 508–515, Nov. 2018, doi: 10.3846/jcem.2018.6186.

[11] J. McKinney and F. Ali, 'Artificial Neural Networks for the Spalling Classification & Failure Prediction Times of High Strength Concrete Columns', *J. Struct. Fire Eng.*, vol. 5, no. 3, pp. 203–214, Sep. 2014, doi: 10.1260/2040-2317.5.3.203.

[12] S. Gupta, 'Using Artificial Neural Network to Predict the Compressive Strength of Concrete containing Nano-silica', *Civ. Eng. Archit.*, vol. 1, no. 3, pp. 96–102, Oct. 2013, doi: 10.13189/cea.2013.010306.

[13] G. Trtnik, F. Kavčič, and G. Turk, 'Prediction of concrete strength using ultrasonic pulse velocity and artificial neural networks', *Ultrasonics*, vol. 49, no. 1, pp. 53–60, Jan. 2009, doi: 10.1016/j.ultras.2008.05.001.

[14] H. N. Muliauwan, D. Prayogo, G. Gaby, and K. Harsono, 'Prediction of Concrete Compressive Strength Using Artificial Intelligence Methods', *J. Phys. Conf. Ser.*, vol. 1625, no. 1, p. 012018, Sep. 2020, doi: 10.1088/1742-6596/1625/1/012018.

[15] I. Ignatov, O. Mosin, and C. Stoyanov, 'Fields in electromagnetic spectrum emitted from human body. applications in medicine', *J. Health Med. Nurs.*, vol. 7, no. 1–22, 2014.

[16] J. M. Lloyd, *Thermal imaging systems*. Springer Science & Business Media, 2013.

[17] H. Choi, B. F. Soeriawidjaja, S. H. Lee, and M. Kwak, 'A convenient platform for real-time non-contact thermal measurement and processing', *Bull. Korean Chem. Soc.*, 2022.

[18] M. Atkins and M. Boer, 'Application of Thermo-Fluidic Measurement Techniques'. Butterworth-Heinemann, 2016.

[19] T. Sakagami and S. Kubo, 'Development of a new non-destructive testing technique for quantitative evaluations of delamination defects in concrete structures based on phase delay measurement using lock-in thermography', *Infrared Phys. Technol.*, vol. 43, no. 3–5, pp. 311–316, 2002.

[20] C. Maierhofer, A. Brink, M. Röllig, and H. Wiggenhauser, 'Quantitative impulse-thermography as non-destructive testing method in civil engineering–Experimental results and numerical simulations', *Constr. Build. Mater.*, vol. 19, no. 10, pp. 731–737, 2005.
[21] H. Wiggenhauser, 'Active IR-applications in civil engineering', *Infrared Phys. Technol.*, vol. 43, no. 3–5, pp. 233–238, 2002.
[22] K. Tomita and M. Y. L. Chew, 'A Review of infrared thermography for delamination detection on infrastructures and buildings', *Sensors*, vol. 22, no. 2, p. 423, 2022.
[23] Y. Cho, N. Bianchi-Berthouze, N. Marquardt, and S. J. Julier, 'Deep Thermal Imaging: Proximate Material Type Recognition in the Wild through Deep Learning of Spatial Surface Temperature Patterns', in *Proceedings of the 2018 CHI Conference on Human Factors in Computing Systems*, Montreal QC Canada, Apr. 2018, pp. 1–13. doi: 10.1145/3173574.3173576.
[24] R. Khallaf and M. Khallaf, 'Classification and analysis of deep learning applications in construction: A systematic literature review', *Autom. Constr.*, vol. 129, p. 103760, Sep. 2021, doi: 10.1016/j.autcon.2021.103760.
[25] T. Drzymała, W. Jackiewicz-Rek, M. Tomaszewski, A. Kuś, J. Gałaj, and R. Šukys, 'Effects of High Temperature on the Properties of High Performance Concrete (HPC)', *Procedia Eng.*, vol. 172, pp. 256–263, 2017, doi: 10.1016/j.proeng.2017.02.108.
[26] D. Andrushia A, A. N, E. Lubloy, and P. A. G, 'Deep learning based thermal crack detection on structural concrete exposed to elevated temperature', *Adv. Struct. Eng.*, vol. 24, no. 9, pp. 1896–1909, Jul. 2021, doi: 10.1177/1369433220986637.
[27] D. G. Aggelis, E. Z. Kordatos, M. Strantza, D. V. Soulioti, and T. E. Matikas, 'NDT approach for characterisation of subsurface cracks in concrete', *Constr. Build. Mater.*, vol. 25, no. 7, pp. 3089–3097, Jul. 2011, doi: 10.1016/j.conbuildmat.2010.12.045.
[28] M. Abuhmida, D. Milne, J. Bai, and M. Sahal, 'ABAQUS-concrete hidden defects thermal simulation'. Mendeley Data, 2022. doi: 10.17632/65nbxg9pr3.1.
[29] G. G. Celano, 'A ResNet-50-based Convolutional Neural Network Model for Language ID Identification from Speech Recordings', in *Proceedings of the Third Workshop on Computational Typology and Multilingual NLP*, 2021, pp. 136–144.
[30] Y. Fang, L. Dong, H. Bao, X. Wang, and F. Wei, 'Corrupted image modeling for self-supervised visual pre-training', *ArXiv Prepr. ArXiv220203382*, 2022.
[31] S. Mascarenhas and M. Agarwal, 'A comparison between VGG16, VGG19 and ResNet50 architecture frameworks for Image Classification', in *2021 International Conference on Disruptive Technologies for Multi-Disciplinary Research and Applications (CENTCON)*, 2021, vol. 1, pp. 96–99.
[32] K. He, X. Zhang, S. Ren, and J. Sun, 'Deep Residual Learning for Image Recognition'.
[33] T. Ridnik, H. Lawen, A. Noy, E. Ben Baruch, G. Sharir, and I. Friedman, 'Tresnet: High performance gpu-dedicated architecture', in *Proceedings of the IEEE/CVF Winter Conference on Applications of Computer Vision*, 2021, pp. 1400–1409.
[34] J. Peng *et al.*, 'Residual convolutional neural network for predicting response of transarterial chemoembolisation in hepatocellular carcinoma from CT imaging', *Eur. Radiol.*, vol. 30, no. 1, pp. 413–424, 2020.
[35] C. Szegedy, V. Vanhoucke, S. Ioffe, J. Shlens, and Z. Wojna, 'Rethinking the inception architecture for computer vision', presented at the Proceedings of the IEEE conference on computer vision and pattern recognition, 2016, pp. 2818–2826.
[36] M.-H. Guo *et al.*, 'Attention mechanisms in computer vision: A survey', *Comput. Vis. Media*, vol. 8, no. 3, pp. 331–368, 2022.
[37] D. Hu, J. Chen, and S. Li, 'Reconstructing unseen spaces in collapsed structures for search and rescue via deep learning based radargram inversion', *Autom. Constr.*, vol. 140, p. 104380, 2022.
[38] M. Abuhmida, D. Milne, J. Bai, and M. Sahal, 'Concrete pressure test- thermal images'. Mendeley Data, 2022. doi: 10.17632/kbvssyjhcj.1.